Supplementary material for LHCb-PAPER-2014-047

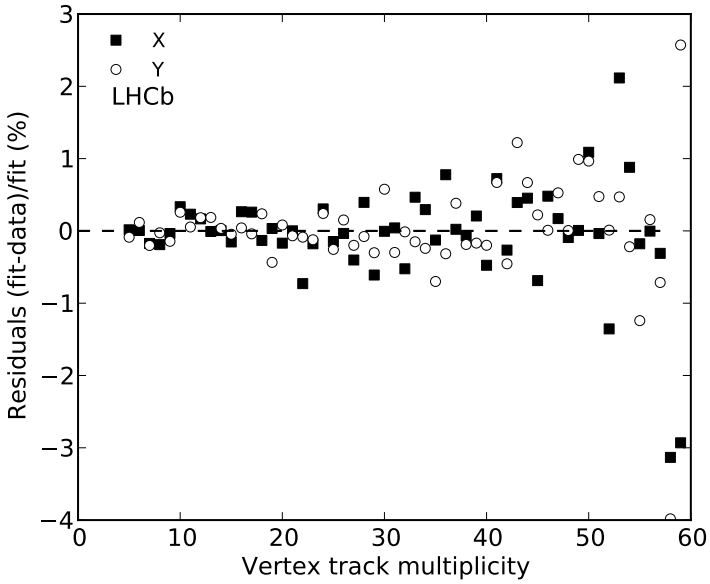

Figure 1: Residuals between parameterization fit and direct resolution measurement for beam-beam interactions (fill 2520). The direct measurement is less precise above about 50 tracks per split vertex where the single Gaussian fits start to be statistically limited.

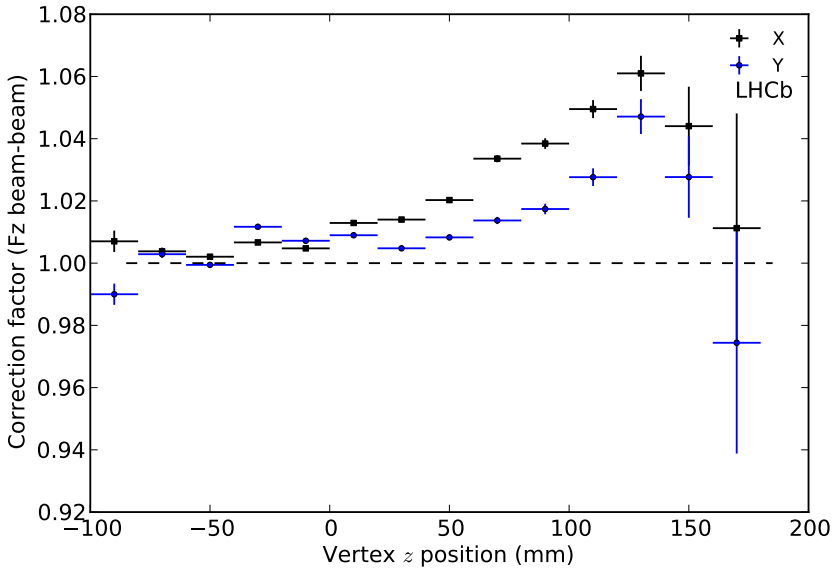

Figure 2: Beam-beam resolution z dependent correction factor F_z based on a resolution parametrization measured in the central z range $z = \pm 5$ mm (fill 2520 with $\beta^* = 3$ m). In the bins near $z = 0$ the values of F_z are not exactly equal to unity due to a binning effect and the fact that here all track multiplicities are accumulated in a single distribution, while the original parametrization was made for each track multiplicity independently.

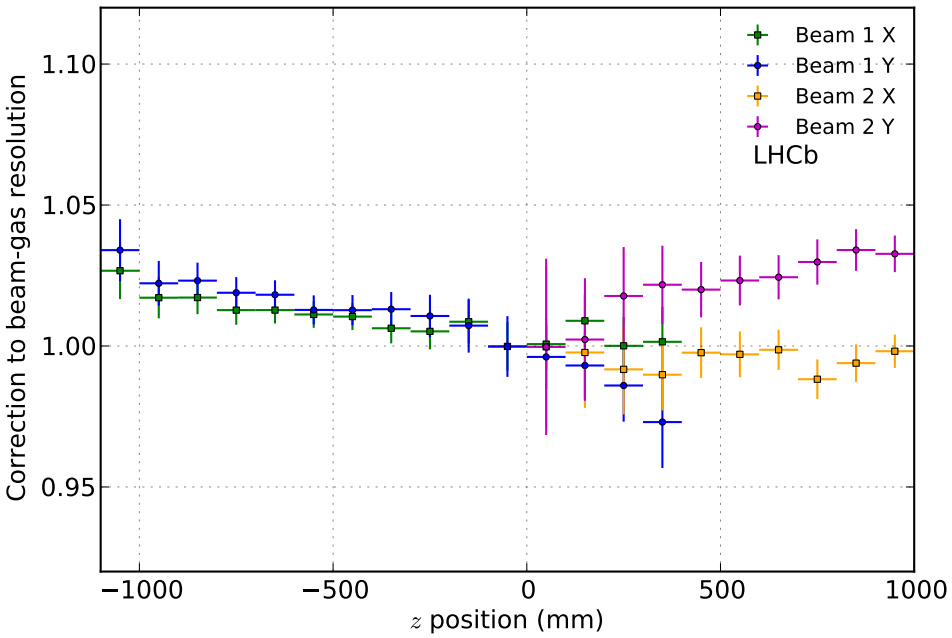

Figure 3: Beam-gas resolution correction factors f_z as function of z (for fill 2520 with $\beta^* = 3$ m).

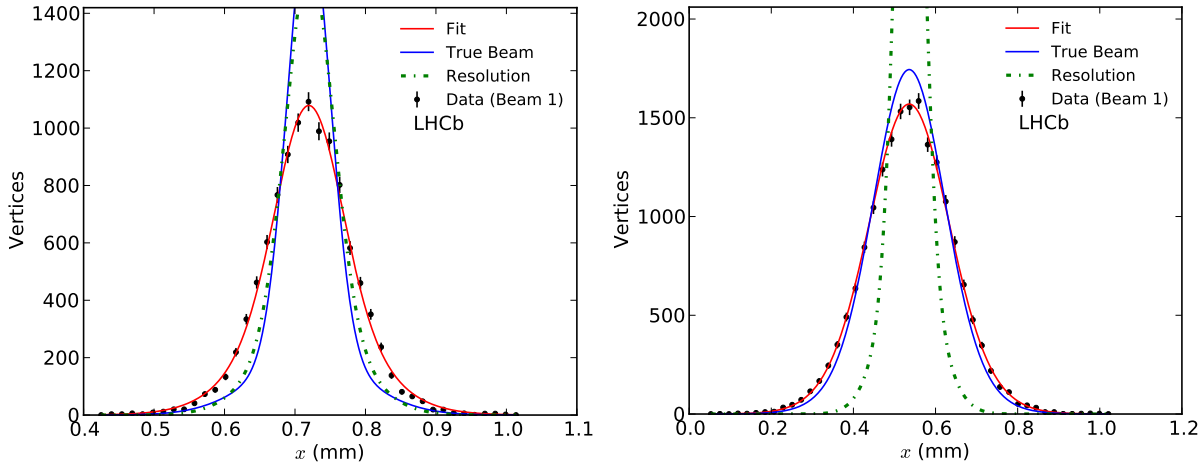

Figure 4: Resolution deconvolution examples. Left: single beam shape measurement of beam 1 in x for fill 2520 with $\beta^* = 3$ m. The true beam width is about 45 µm. Right: single beam shape measurement of beam 1 in x for fill 2852 with $\beta^* = 10$ m. The true beam width is about 93 µm. Both measurements assume a double Gaussian beam shape and are performed on the most central z slice using vertices in the range $-500 < z < -250$ mm. The SMOG gas injection was active; the number of vertices in the distributions is about 10^4 and 1.4×10^4 for the left and right plot, respectively.

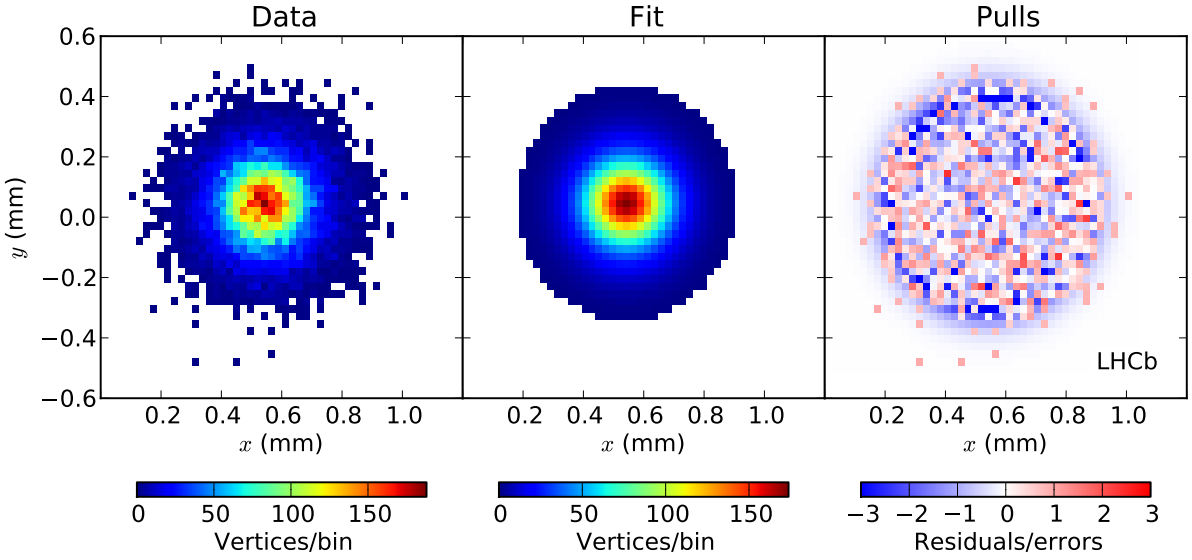

Figure 5: Example of a z slice fit result in 2-dimensions showing a single beam transverse projection for BCID 1909 in fill 2853. Left panel: raw beam transverse distribution; each square has a color proportional to the number of vertices it contains. Central panel: fit predictions including resolution convolution. Right panel: Pulls of the fit in the range [-3,3] as defined by $\text{pulls}_{i,j} = \frac{N_{i,j} - f(x_i, y_i)}{\sqrt{N_{i,j}}}$.

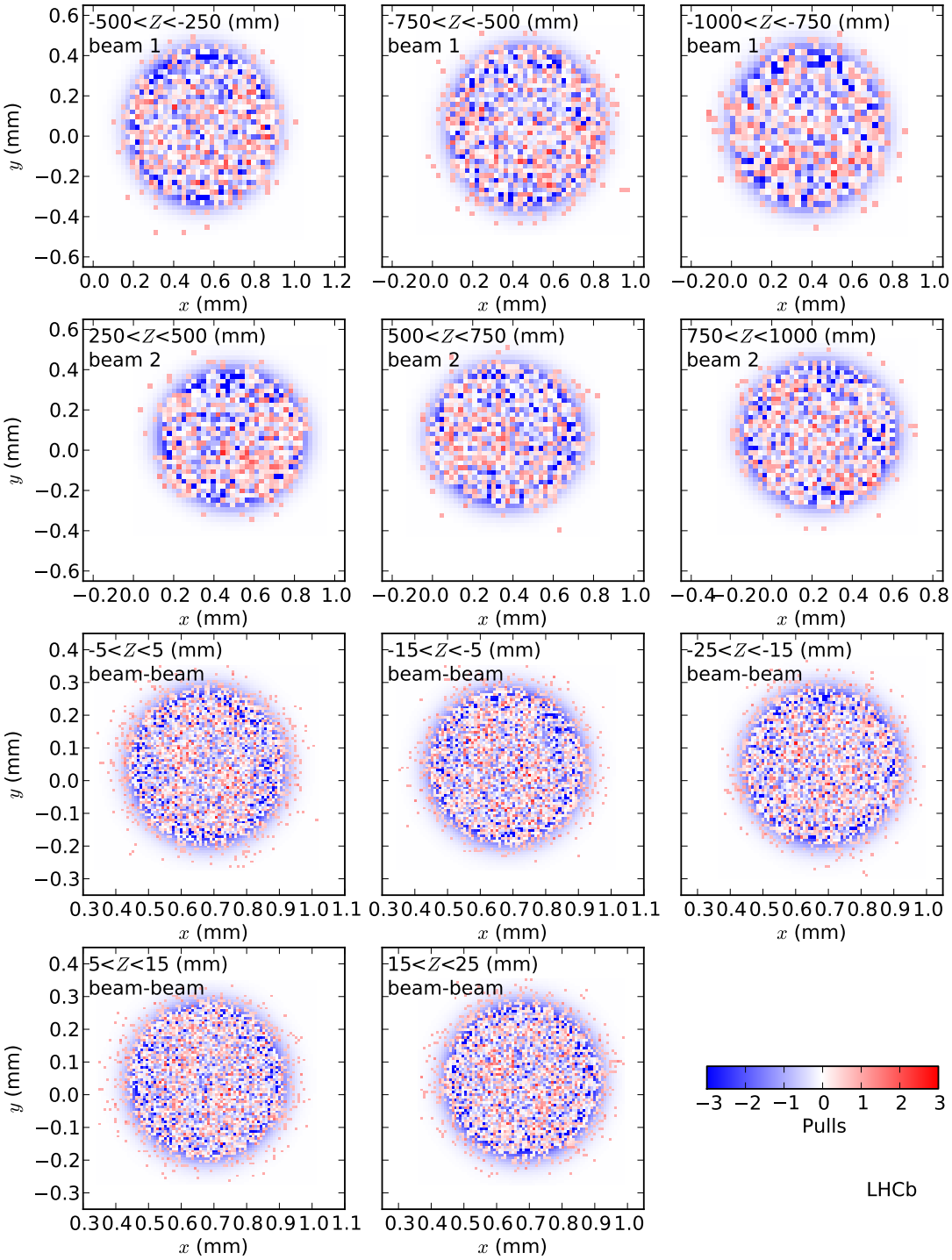

Figure 6: Global fit results of a colliding bunch pair in 2-dimensions showing the fit pulls for fill 2853. The same z slices as shown in Fig. **??** are shown here with the two-dimensional fit. The z range and collision type of each distribution is indicated in the plots. The first three panels show the fit results of the three beam 1 z slices, the next three slices are for beam 2, the remaining five distribution show the central beam-beam slices (the remaining 13 slices used in the fit are not shown for better readability). The pulls are evaluated with $\text{pulls}_{i,j} = \frac{N_{i,j} - f(x_i, y_i)}{\sqrt{N_{i,j}}}$.

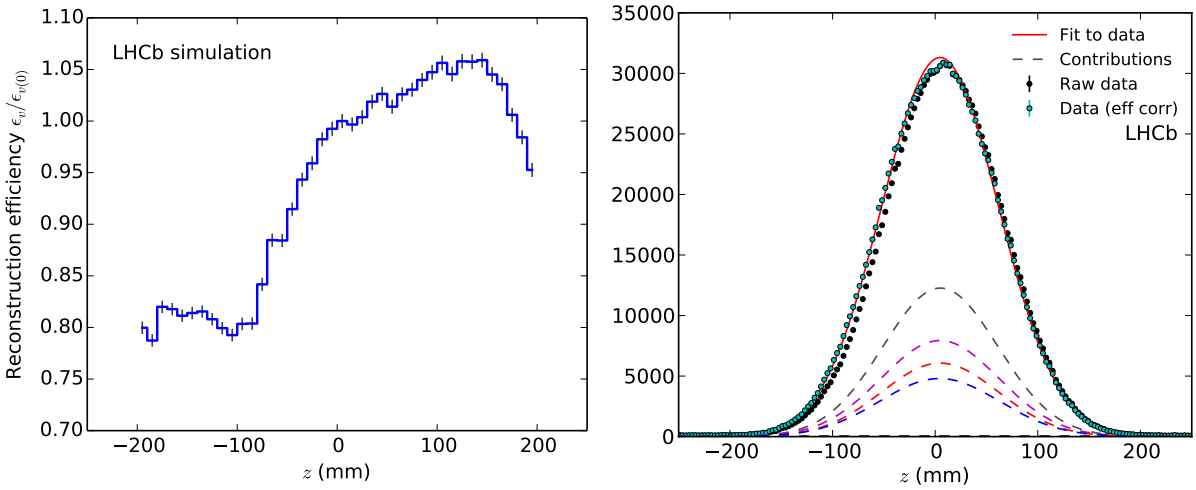

Figure 7: Left: relative vertex reconstruction efficiency as function of z for pp collisions at $\sqrt{s} = 8$ TeV. The 100% efficiency is set at $z = 0$ as to keep the amplitudes between raw and corrected data similar; however, the absolute scale of the correction does not change the fit results. Right: fit of the longitudinal vertex distribution of a colliding bunch pair (BCID 1335) after reconstruction efficiency correction for fill 2855. The solid red line is the fit result. The different contributions to the final fit shape are shown as dashed lines.

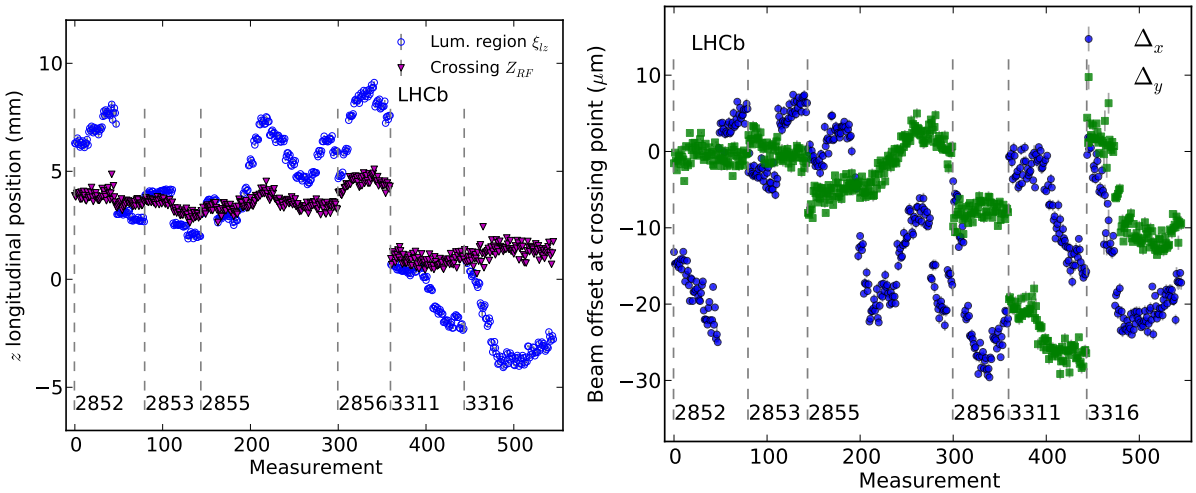

Figure 8: Left: Longitudinal z position of the luminous region center and bunch crossing point z_{rf}. Each data point is one measurement period for one colliding BCID. The measurements are sorted by time and BCID. While the luminous region z position will move as beams drift in the crossing plane, the crossing point z_{rf} is determined by the stability of the LHC RF cavities and is expected to be constant within ± 2 mm within a fill but can have larger differences over a longer period as is seen between the first 4 fills in July and the last 2 fills in November. The statistical uncertainty is smaller than the marker. Right: beam offset in x and y at the crossing point z_{rf}.

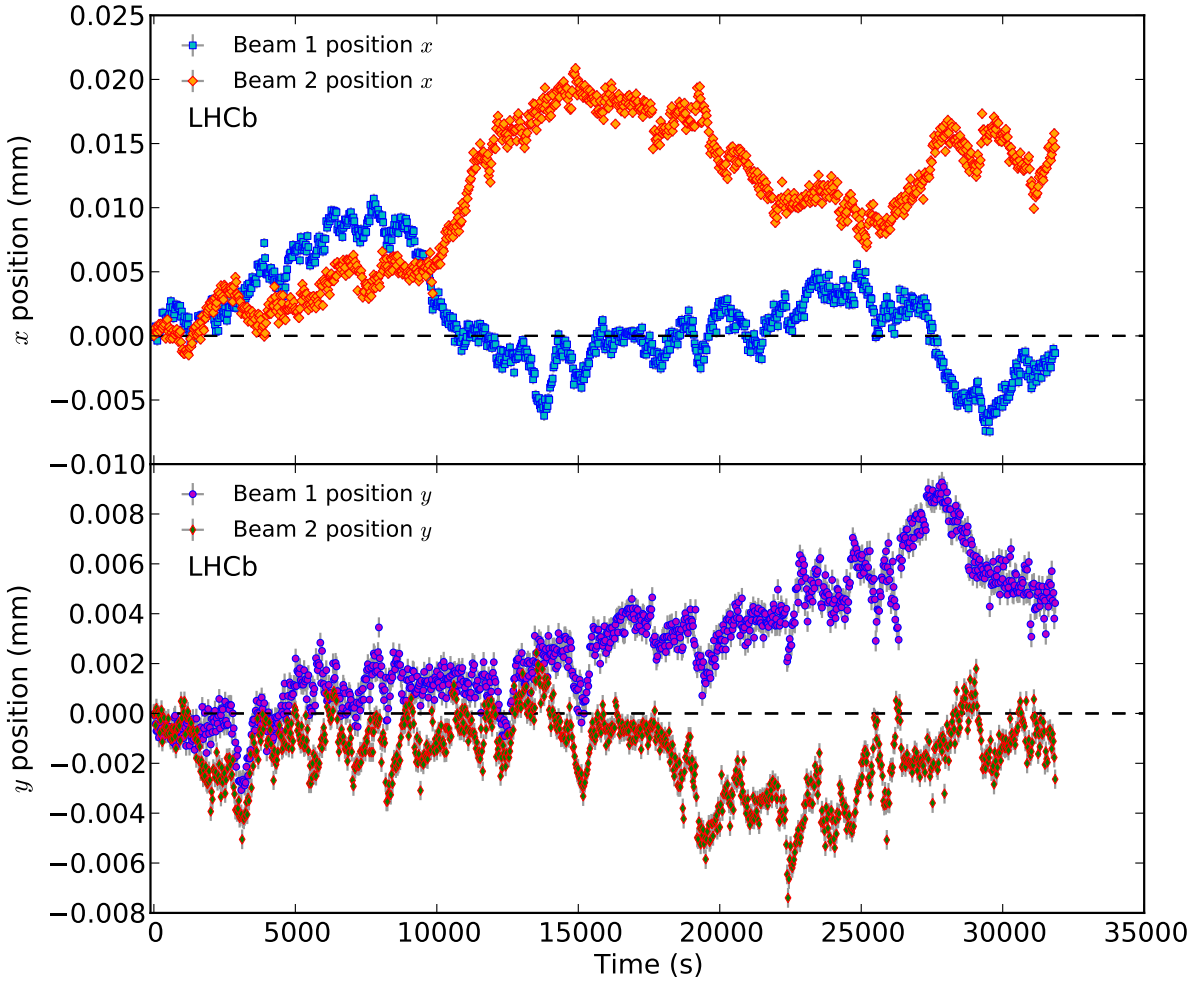

Figure 9: Single beam orbit drift measurement measured during fill 2855 which stayed about 9 hours in Stable Beams. The absolute position is set at zero on the first measurement to better compare the relative drift over time. Each point is measured over a time period of 30 seconds using beam-gas interaction vertices from all bunches. Top panel: measured x position. Bottom panel: measured y position. The indicated errors are statistical only with a typical accuracy of about 0.3 µm.

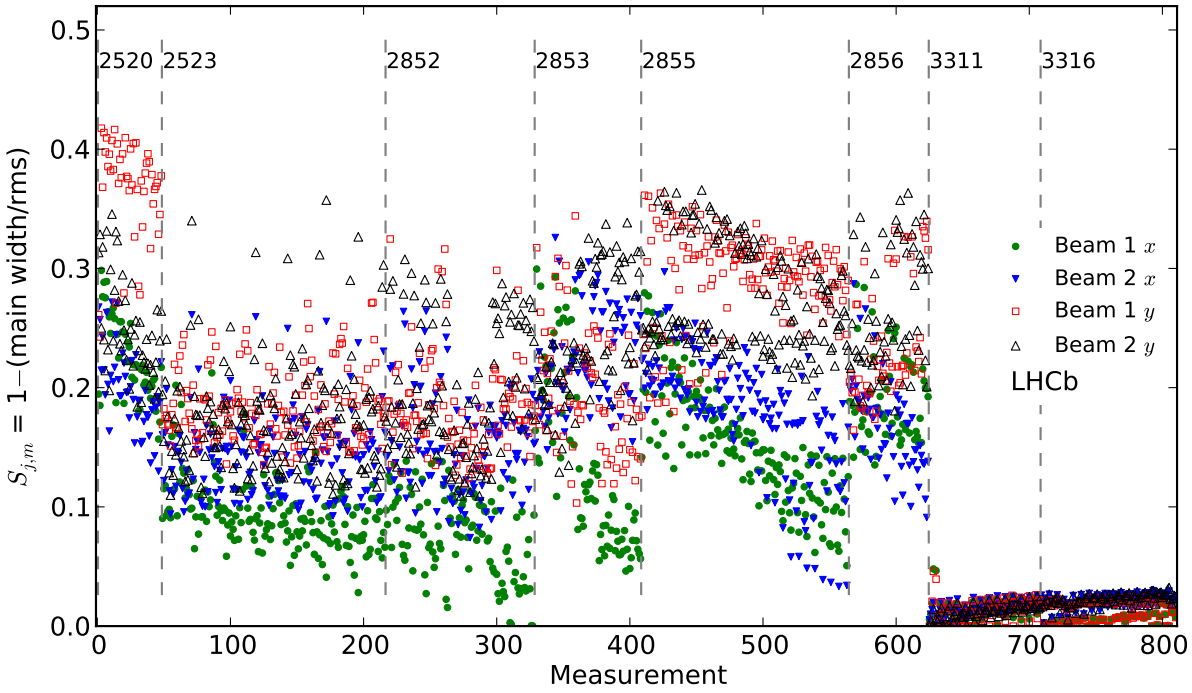

Figure 10: Strength of double Gaussian beam shape for all measurements performed in 2012 at $\sqrt{s} = 8$ TeV sorted by time and BCID. The different fills are indicated by a vertical dashed line. A single Gaussian shape would have a strength of zero. Both November fills (3311 and 3316) are described with the same double Gaussian function as for the other fills but the narrow component can have a negative weight.

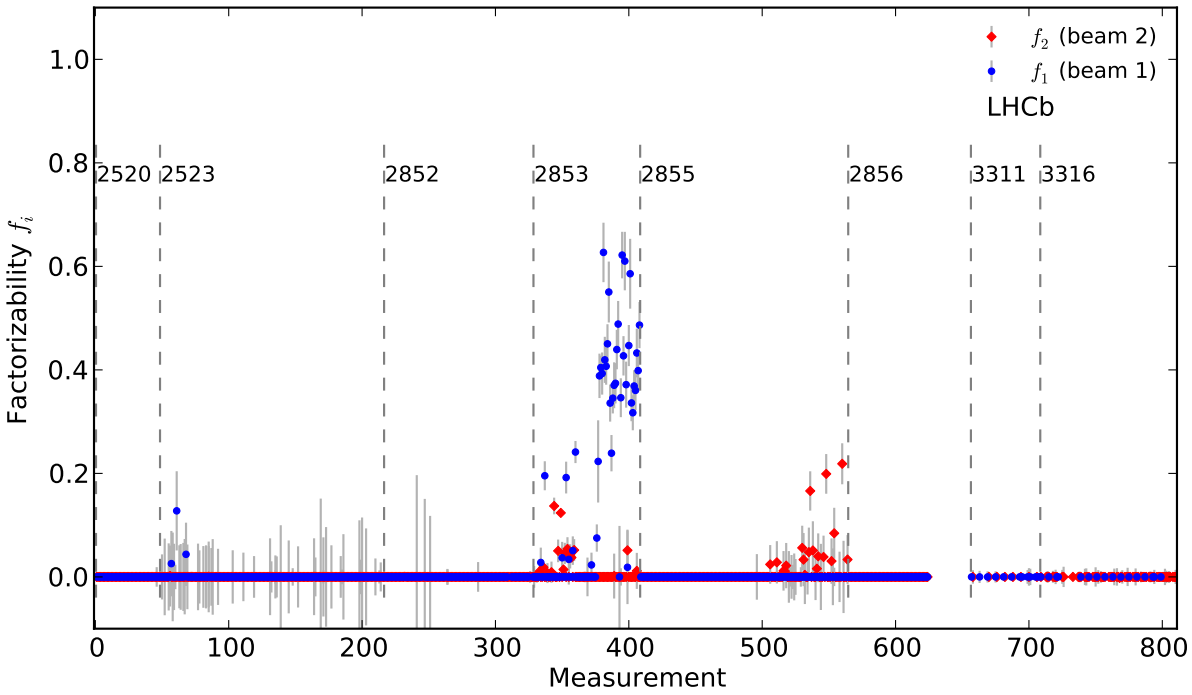

Figure 11: Measurement of beam factorizability for all measurements performed in 2012 at $\sqrt{s} = 8$ TeV sorted by time and BCID. Only f_j values are shown for which the double Gaussian strength $S_{j,m}$ was larger than 0.02 and the uncertainty on the factorizability parameter $\delta(f_j)$ was smaller than 1.

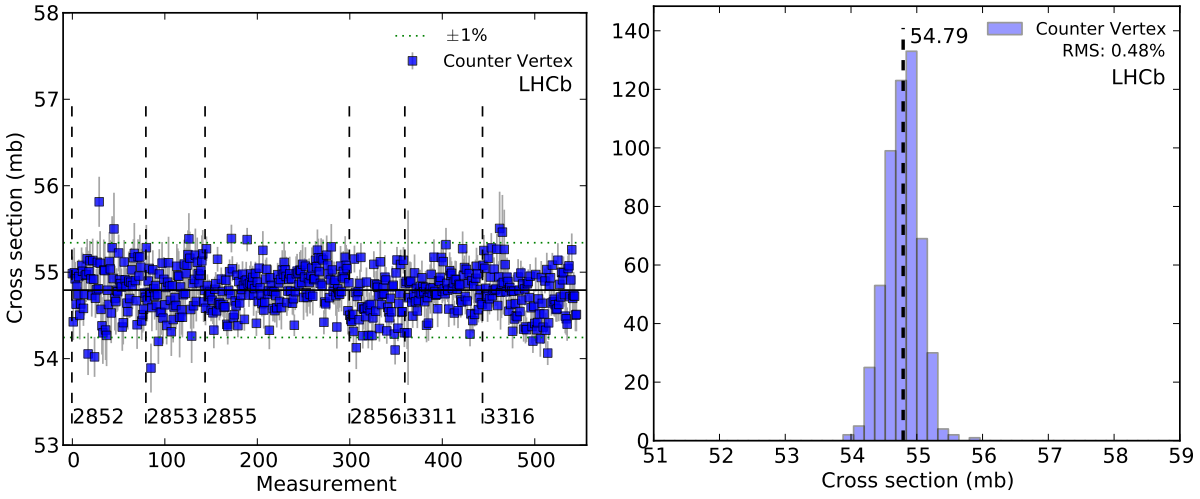

Figure 12: Cross-section results for head-on beam periods with $\beta^* = 10$ m fills at $\sqrt{s} = 8$ TeV after FBCT offset correction. Left: cross-section measurement per colliding bunch pair and 20 minutes time integration. The measurements are sorted by time and BCID; the different fills are separated by a dashed vertical line and indicated in the figure. Two dotted horizontal lines show the ±1% deviation from the central value. Right: histogram of all cross-section measurement from the left plot, the measurement spread is reduced from 0.54% to 0.48% after FBCT offset correction; however, the cross-section is not changed significantly by the FBCT offset fit. The median value is indicated by a dashed vertical line.

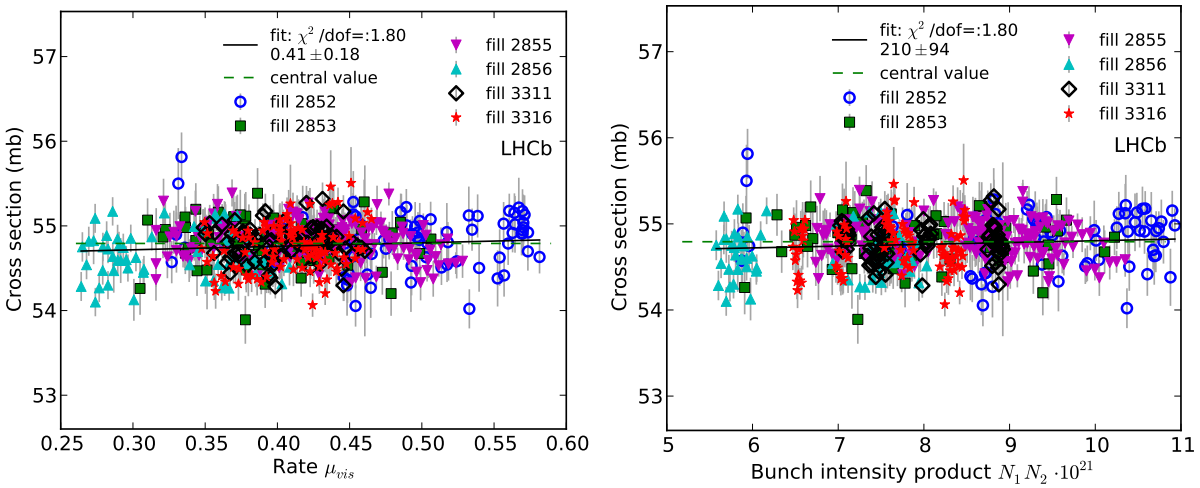

Figure 13: Left: cross-section correlation with the average interaction rate per crossings $\mu_{\rm ref}$. Right: cross-section correlation with the bunch intensity product $N_1 N_2$. The central value is indicated as dashed horizontal line. A straight line fit through all data points is shown as solid black line.

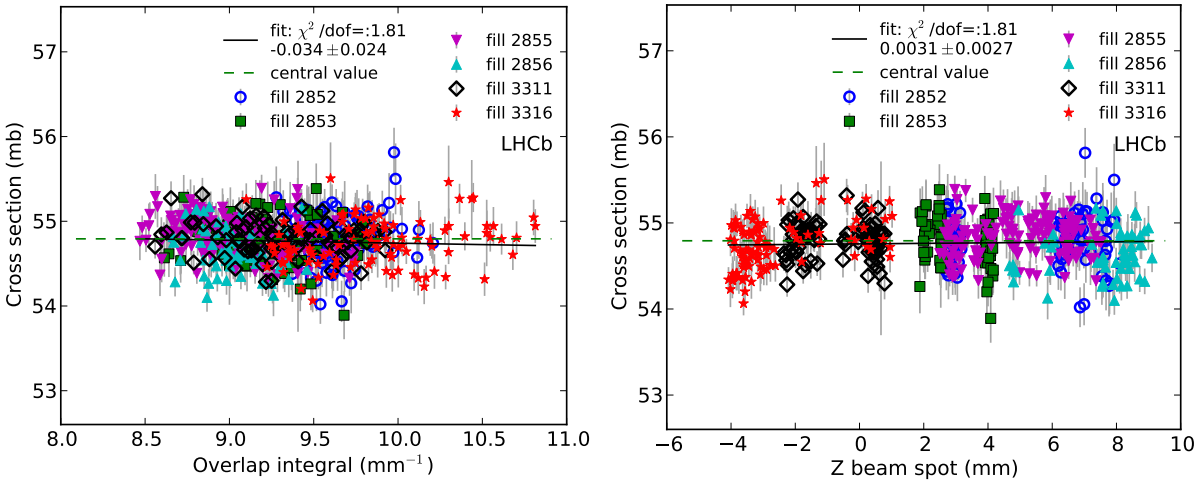

Figure 14: Left: cross-section correlation with the overlap integral. Right: cross-section correlation with the luminous region z centre. The central value is indicated as dashed horizontal line. A straight line fit through all data points is shown as solid black line.

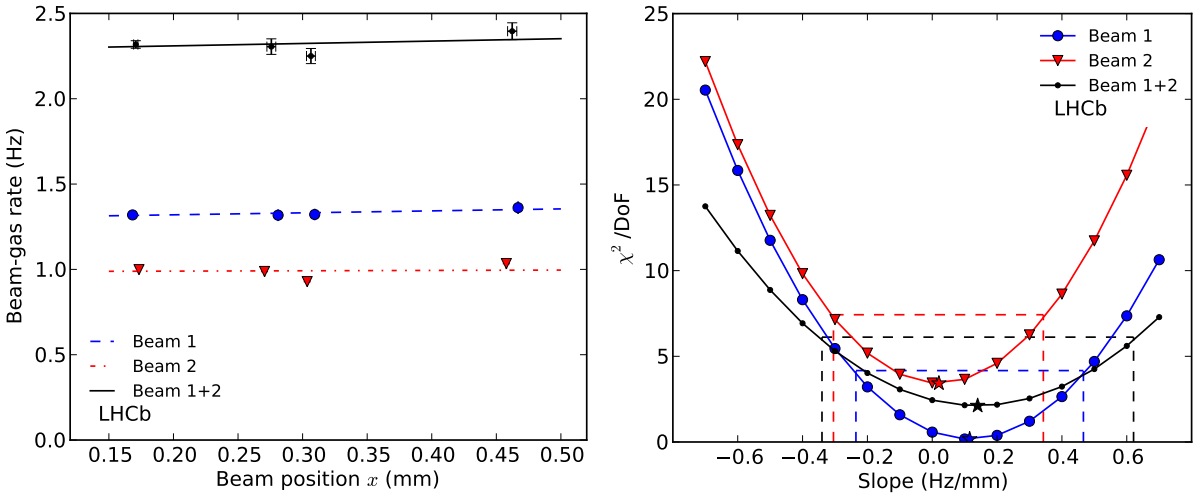

Figure 15: Left: measurement of pressure gradient in the VELO. Right: χ^2 analysis on the gradient to set a limit on a transverse pressure gradient.

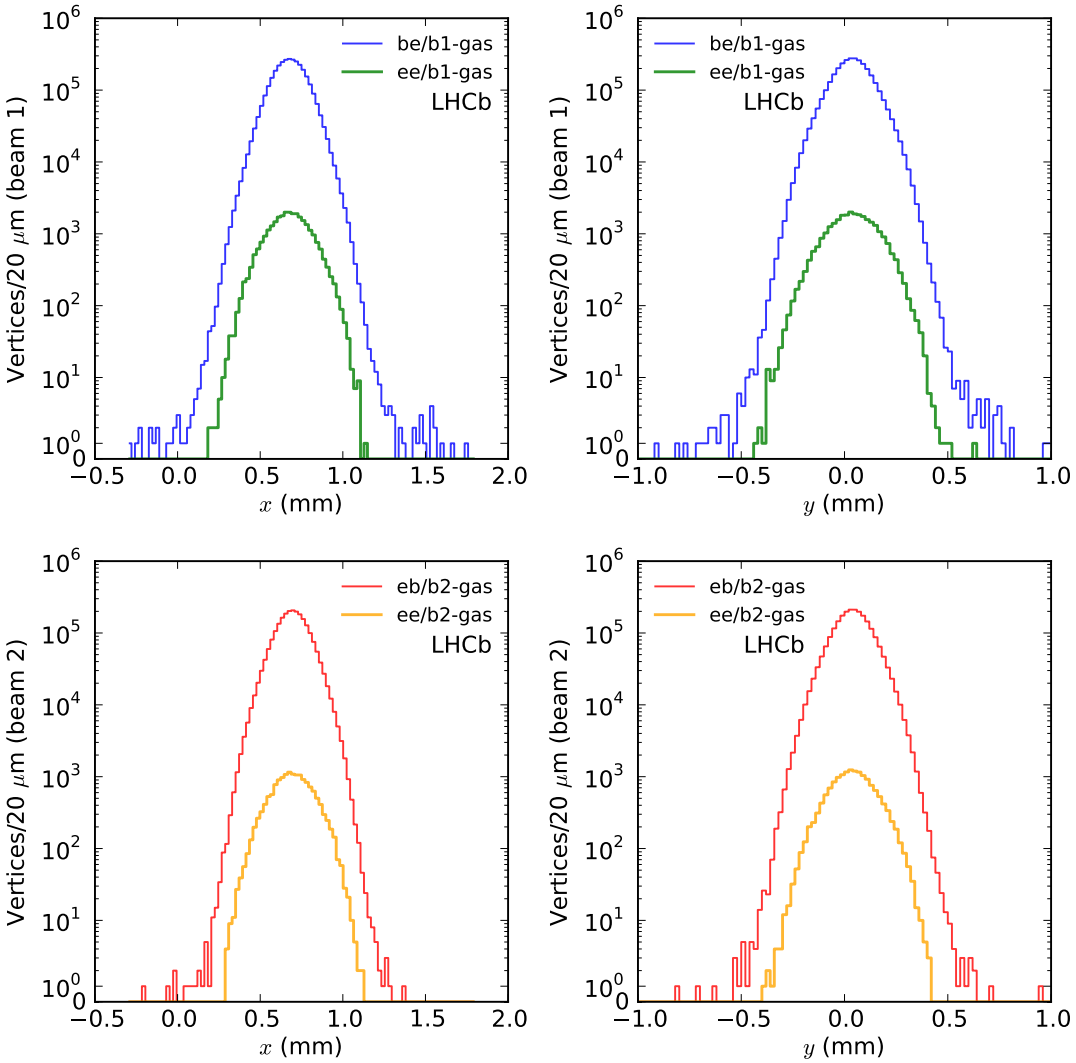

Figure 16: Transverse distribution of selected beam-gas events for ghost charge analysis. All vertices are projected along the corresponding beam direction onto the x-y plane. Histograms from beam 1 vertices are on both top panels and from beam 2 on both bottom panels. The less populated histograms are from ee events of the corresponding beam.

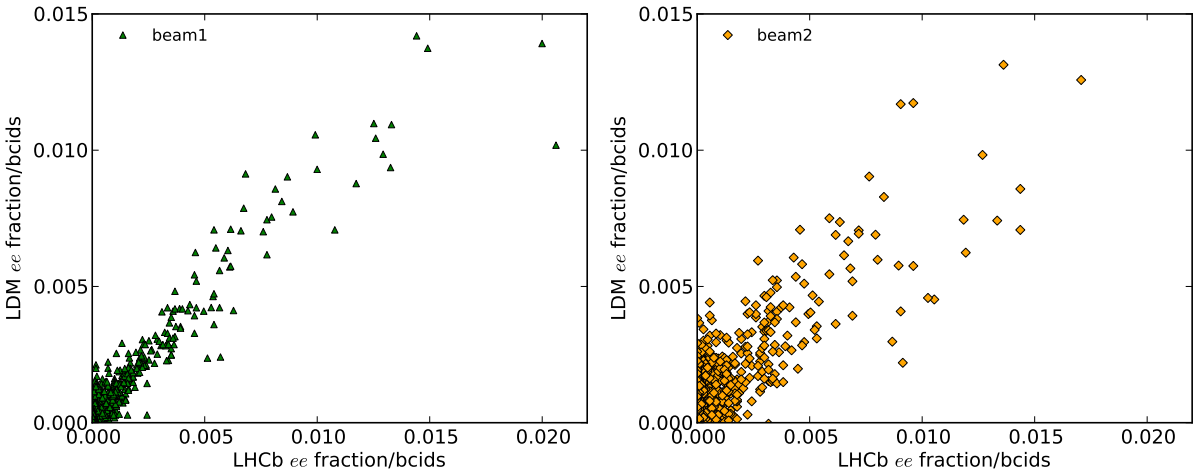

Figure 17: Correlation between ghost charge fractions measured by the LDM and LHCb for fill 2853. Each data point corresponds to one BCID measurement, the values are normalized such that the sum of all data points per beam is equal to one.

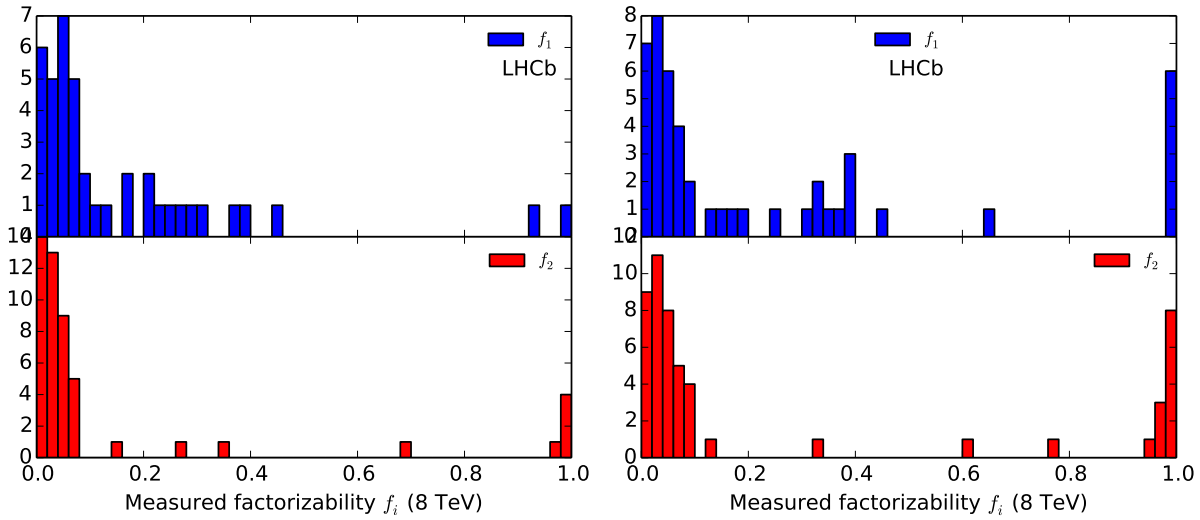

Figure 18: Fit results for factorizability parameters $f_{1,2}$ for all measurements performed in 2011 at $\sqrt{s} = 8$ TeV. Only bunch pairs with a double Gaussian strength $S_{j,m} > 0.02$ and with a fit uncertainty on the factorizability parameter of $\delta(f_j) < 1$ are displayed. Left: fit results using the full dataset. Right: fit results using the high track multiplicity cut that reduces the number of vertices to about half the full dataset. Top panels: beam 1. Bottom panels: beam 2